

Article

Investigation of Optimal Light Source Wavelength for Cuffless Blood Pressure Estimation Using a Single Photoplethysmography Sensor

Sogo Toda ^{1,*}  and Kenta Matsumura ² 

¹ Ishikawa College, National Institute of Technology, Tsubata 929-0392, Japan

² Faculty of Medicine, University of Toyama, Toyama 930-0194, Japan

* Correspondence: s-toda@ishikawa-nct.ac.jp

Abstract: Routine blood pressure measurement is important for the early detection of various diseases. Recently, cuffless blood pressure estimation methods that do not require cuff pressurization have attracted attention. In this study, we investigated the effect of the light source wavelength on the accuracy of blood pressure estimation using only two physiological indices that can be calculated with photoplethysmography alone, namely, heart rate and modified normalized pulse volume. Using a newly developed photoplethysmography sensor that can simultaneously measure photoplethysmograms at four wavelengths, we evaluated its estimation accuracy for systolic blood pressure, diastolic blood pressure, and mean arterial pressure against a standard cuff sphygmomanometer. Mental stress tasks were used to alter the blood pressure of 14 participants, and multiple linear regression analysis showed the best light sources to be near-infrared for systolic blood pressure and blue for both diastolic blood pressure and mean arterial pressure. The importance of the light source wavelength for the photoplethysmogram in cuffless blood pressure estimation was clarified.

Keywords: blood pressure; heart rate; modified normalized pulse volume; optical wavelength; photoplethysmography



Citation: Toda, S.; Matsumura, K. Investigation of Optimal Light Source Wavelength for Cuffless Blood Pressure Estimation Using a Single Photoplethysmography Sensor. *Sensors* **2023**, *23*, 3689. <https://doi.org/10.3390/s23073689>

Academic Editors: Mimma Nardelli and Raquel Bailón

Received: 24 February 2023

Revised: 30 March 2023

Accepted: 30 March 2023

Published: 2 April 2023



Copyright: © 2023 by the authors. Licensee MDPI, Basel, Switzerland. This article is an open access article distributed under the terms and conditions of the Creative Commons Attribution (CC BY) license (<https://creativecommons.org/licenses/by/4.0/>).

1. Introduction

High arterial blood pressure (BP) is known worldwide as a risk factor for various diseases, including cardiovascular disease [1–3]. Because BP can change significantly in a short period of time, it is important to measure it frequently for routine health monitoring [4,5]. Therefore, routine BP measurement methods must be noninvasive and simple. Currently, the most widely used BP measurement method is the cuff-based BP measurement method, which is based on either the oscillometric method [6] or the Riva-Rocci-Korotkov method [7]. Although cuff-based BP measurement is noninvasive and highly accurate, the cuff must be attached to the upper arm, wrist, or fingers and then pressurized; this causes discomfort during measurement and means that the method is unsuitable at certain times, including during sleep.

To address this problem, “cuffless BP”—a method of BP estimation that does not require cuff pressurization—has been explored [8–25]. The advantages of cuffless BP are that it eliminates the inconvenience and discomfort of pressurization and does not require a pressurization device, thereby allowing the measurement device to be simplified and downsized. These advantages make cuffless BP suitable for measurement at any time. Various methods have been proposed for cuffless BP estimation, including methods based on pulse transit time (PTT) [8–18]; methods using feature values of PTT, photoplethysmograms (PPGs), and electrocardiograms (ECGs); and methods using pressure sensors and PPG [19–25]. Typical PTT-based methods include those that perform PPG measurements at two different locations to obtain the PTT and those that use the time shift between the ECG and PPG peaks [9]. It is known that there is a positive correlation between PTT and

BP [26]. To estimate BP from the PTT, there are methods that approximate the relationship between them using a linear model [10], a logarithmic model [11], or an inverse-square model [12]; a method using the Hilbert–Huang transform used in signal processing [13]; and a nonlinear second-order curve-fitting regression model [14]. All of these methods require calibration using a cuff sphygmomanometer [17,18]. Other cuffless BP estimation methods include those that estimate BP from ECG and PPG features [19,20] and those that estimate BP from PPG features alone with machine learning [21,22]. Moreover, the method of using a pressure sensor and a PPG requires the fingertip to be pressed into the pressure sensor, which makes the measurement burdensome [23].

Instead, we have studied a method for estimating BP from a single PPG based on findings from circulation physiology and psychophysiology [24,25]. This method uses the fact that BP is expressed as the product of cardiac output (CO) and total peripheral resistance (TPR) [27]. Furthermore, the CO and TPR required for BP estimation can be approximated using the heart rate (HR) and the modified normalized pulse volume (mNPV) obtained from the PPG, respectively [28–32]. Therefore, BP can be estimated from the product of HR and mNPV. Using this method, BP is estimated by calculating the mNPV and HR from the obtained PPG and so can be realized using a single PPG, and thus, BP can be estimated with a certain degree of accuracy using only the built-in flashlight and CMOS camera of a smartphone [25].

The proposed method performs BP estimation using a single PPG, but in previous studies, the light source used for PPGs has generally been restricted to near-infrared (NIR) light [25]. NIR and green light are the most common light sources used for PPGs, but the optical properties of biological tissues mean that the longer the wavelength, the deeper the penetration into the body and the different tissues that are passed through [33–35]. Therefore, it is possible that different light source wavelengths may cause different types of blood vessels to be observed. Although CO does not change depending on the vessels observed, TPR may change. Thus, the estimated BP may differ depending on the wavelength used. Therefore, it is necessary to investigate the wavelength characteristics of the PPG light source for the proposed method in order to study the fundamental characteristics of this method. BP estimation at multiple PPG wavelengths can provide information on the optimal wavelength, but BP can vary widely from second to second. Therefore, we measured PPGs at multiple wavelengths simultaneously and used them to estimate BP using the proposed method. Our aim was to investigate the optimal wavelength by comparing the estimated BP with that measured using a cuff sphygmomanometer. This is the first study to focus on the wavelength used for PPGs in cuffless BP estimation.

2. Materials and Methods

2.1. PPG Measurement

Photoplethysmography involves obtaining waveforms of changes in the volume of blood vessels by using the optical absorption characteristics of blood [36,37]. It is performed using a noninvasive and compact device because measurements are made using only a light source and a photodetector. There are 2 PPG measurement modes: the reflectance mode, in which the light source and photosensor are placed on the same side of the measurement site, and the transmittance mode, in which they are placed on opposite sides. The PPG measurement site is a fingertip, wrist, or earlobe.

In this study, we constructed a multiwavelength PPG sensor, as shown in Figure 1, to measure multiwavelength PPGs simultaneously. For the light sources, we used 4 light-emitting diodes (LEDs), namely, an NIR LED (870 nm; SIM-040ST), a red LED (620 nm; SML-Z14U4T), a green LED (528 nm; SMLZ14EGT), and a blue LED (470 nm; SMLZN4BGT) (all from ROHM Semiconductor, Kyoto, Japan), and as the photodetector, we used a photodiode (TEMD5510; Vishay Semiconductors, Malvern, PA, USA). Because blue and green cannot be measured in transmittance mode, our developed PPG sensor operates in reflectance mode. As shown in Figure 2, to measure multiwavelength PPGs simultaneously,

the 4 LEDs were chopper-emitted, and the light intensity of each was adjusted so that it was the same after propagation through the fingertip.

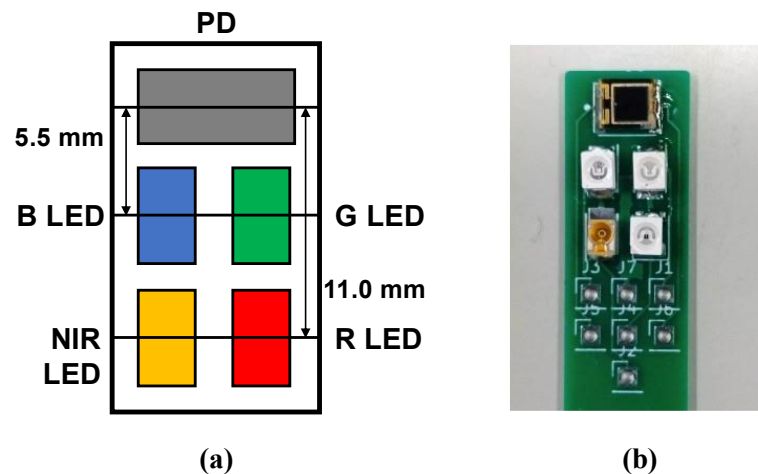


Figure 1. Developed multiwavelength photoplethysmogram (PPG) sensor: (a) layout of light-emitting diodes (LEDs) and photodiode (PD). B LED = blue LED (470 nm), G LED = green LED (528 nm), R LED = red LED (620 nm), and NIR LED = near-infrared LED (870 nm); (b) actual PPG sensor.

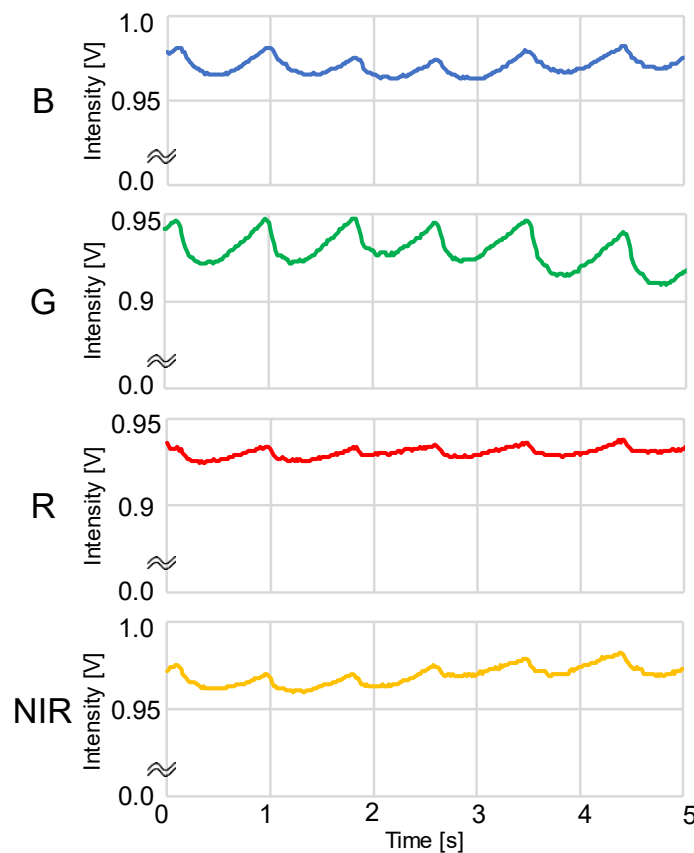


Figure 2. Example of simultaneous recordings of blue, green, red, and near-infrared light photoplethysmograms (PPGs) measured using a DC amp: B = blue LED PPG, G = green LED PPG, R = red LED PPG, and NIR = near-infrared LED PPG.

The PPGs were obtained by sampling at a frequency of 60 Hz, performing analog-to-digital conversion using a microcontroller (mbed LPC1768; ARM, Cambridge, UK), and then importing the data into a computer. The PPG waveforms were processed as shown in Figure 3 using the LabVIEW 2020 software (version 20.0f1 (32-bit)), and the AC component,

DC component, and peak interval (T) of the waveforms were averaged to obtain the HR and mNPV. The HR was obtained from the peak interval T of the PPG as $HR = 60/T$, and the mNPV was calculated from the AC/DC ratio of the PPG. During the waveform analysis, positions where maxima continued or where T was extremely short or long were removed as outliers.

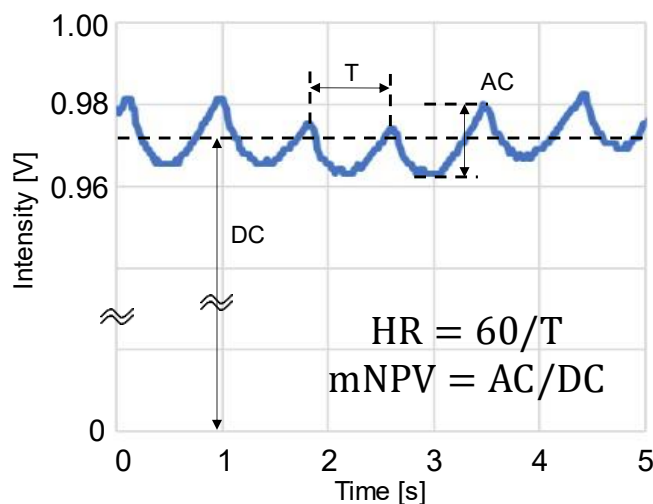


Figure 3. Schematic of photoplethysmogram (PPG) waveform feature values: AC is the amplitude of PPG, DC is the mean value of PPG, T is the peak interval time, HR = heart rate, and mNPV = modified normalized pulse volume [31].

2.2. Cuffless BP Estimation Method

BP is calculated using CO and TPR as $BP = CO \times TPR$ [27]. Taking the natural logarithm (\ln) of both sides of this equation gives $\ln BP = \ln CO + \ln TPR$, and so BP can be regarded as a simple linear polynomial. Furthermore, CO and HR are correlated because they are both affected by β -adrenergic sympathetic nerve activity [28,29]. Similarly, TPR and mNPV are correlated because they are both affected by α -adrenergic sympathetic nerve activity [30–32]. Therefore, the equation

$$\ln BP = \ln HR + \ln mNPV \quad (1)$$

holds, which shows that BP can be estimated using only the HR and mNPV obtained from a single PPG measurement [25]. The same idea applies to systolic BP (SBP), diastolic BP (DBP), and mean arterial pressure (MAP).

2.3. Experimental Protocol

In this study, we investigated how the wavelength of the light source affects the proposed method by measuring BP simultaneously with both a cuff sphygmomanometer and the 4-wavelength PPGs obtained using the multiwavelength PPG sensor shown in Figure 1.

The experiment was conducted in a conference room where the temperature was kept at 20–24 °C. Each participant sat at rest in a chair with both hands on a desk in front of them. A PPG sensor was attached to the index finger of each participant's left hand, and a cuff sphygmomanometer (HCR-7601T; OMRON Healthcare, Kyoto, Japan) was attached to their upper right arm. The PPG sensor was attached to the tip of the participant's index finger using tape to ensure that all 4 LEDs and the PD were in contact with the finger without loosening and that the participant did not feel pressure. The finger with the PPG sensor and the upper arm with the cuff were supported at heart level. The participant was instructed to remain as still as possible during the measurement to reduce the effects of motion artifacts.

As shown in Figure 4, the experiment began with a 3 min baseline (BL) measurement after a sufficient adaptation period. During BL, PPGs were measured constantly, and the cuff sphygmomanometer was used twice, once at the start of measurement and then 90 s thereafter. Next, the participant performed a 3 min mental arithmetic task (MA) in which they were instructed to continuously subtract a number (e.g., keep subtracting 13 from 3000) and to do it as quickly and accurately as possible. During the MA period, PPGs and BP were measured at the same times as they were during the BL period. To calculate the HR and mNPV for the BP estimation with the PPG, we used the PPG waveform from the start of the cuff-sphygmomanometer measurement to 30 s thereafter. However, because the PPG included motion artifacts due to cuff pressure, the waveform during the first 2 s of measurement was removed.

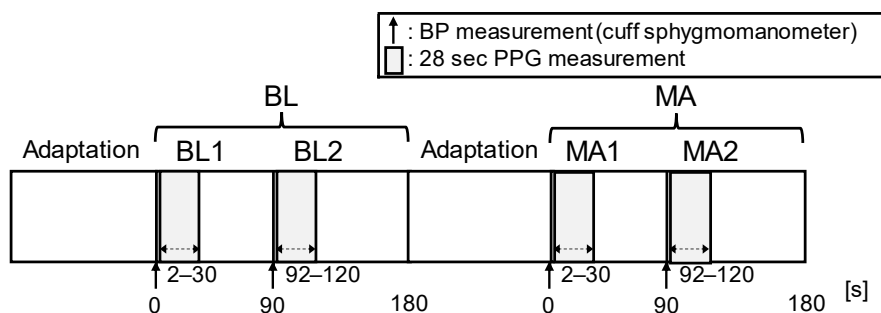


Figure 4. Experimental protocol. The experiment consisted of 2 periods: baseline (BL) and mental arithmetic (MA). Each period lasted 180 s. A total of 2 BP measurements and a PPG measurement (28 s) were taken for each period. The BL period measured the resting condition, and the MA period measured the stress condition induced via mental arithmetic.

2.4. Participants

In total, 14 volunteers (6 Japanese women and 8 Japanese men, aged 19–21 years (19.4 ± 0.6 (mean \pm standard deviation))) were recruited from within Ishikawa College and participated in this study. To do so, volunteers had to be at least 18 years old and free of cardiovascular disease at the time of the experiment. The BPs of the participants measured with a cuff sphygmomanometer are summarized in Table 1. According to the criteria of the American Heart Association [38], there were 2 participants with hypertension stage 1 (130/90 mmHg) and 2 participants with hypotension (90/60 mmHg). For participating, each participant received approximately USD 30. After explaining the details of this study to the participants, written informed consent was obtained. This study was approved by the ethics committee of the National Institute of Technology of Ishikawa College (IRB number: N.A.) on 13 November 2019 and was conducted in accordance with the principles expressed in the Declaration of Helsinki.

Table 1. Participants' BPs measured with a cuff sphygmomanometer in each measurement condition.

Condition	SBP [mmHg]		DBP [mmHg]		MAP [mmHg]	
	Mean	SD	Mean	SD	Mean	SD
BL	112.3	12.3	68.5	6.3	83.1	7.2
MA	121.6	14.2	77.9	8.7	92.5	9.4

BP = blood pressure, SBP = systolic BP, DBP = diastolic BP, MAP = mean arterial pressure, mean = average of BP, SD = standard deviation of BP, BL = baseline (resting condition), MA = mental arithmetic (stress condition induced via mental arithmetic), and $N = 14$.

The sample size of this study was relatively small ($N = 14$) because previous studies on BP estimation based on pulse wave velocity and PPGs have shown that a small number of participants is acceptable unless there is a specific reason indicating otherwise, such as the use of machine learning. For example, Payne et al. [15] used $N = 12$, Patzak et al. [16] used $N = 12$, and the previous study on the proposed method used $N = 13$ [25].

2.5. Data Analysis

Figure 5 shows a flowchart of BP estimation with this method. As shown in Figure 4, 4 BP measurements were taken per participant, 2 in BL (BL1 and BL2) and 2 in MA (MA1 and MA2). The HR and mNPV for each beat were calculated from the PPG waveform at 2–30 s from the start of the BP measurement and averaged. Then, the natural logarithms of HR ($\ln \text{HR}_{\text{BL}1}$, $\ln \text{HR}_{\text{BL}2}$, $\ln \text{HR}_{\text{MA}1}$, and $\ln \text{HR}_{\text{MA}2}$), mNPV ($\ln \text{mNPV}_{\text{BL}1}$, $\ln \text{mNPV}_{\text{BL}2}$, $\ln \text{mNPV}_{\text{MA}1}$, and $\ln \text{mNPV}_{\text{MA}2}$), SBP ($\ln \text{SBP}_{\text{BL}1}$, $\ln \text{SBP}_{\text{BL}2}$, $\ln \text{SBP}_{\text{MA}1}$, and $\ln \text{SBP}_{\text{MA}2}$), DBP ($\ln \text{DBP}_{\text{BL}1}$, $\ln \text{DBP}_{\text{BL}2}$, $\ln \text{DBP}_{\text{MA}1}$, and $\ln \text{DBP}_{\text{MA}2}$), and MAP ($\ln \text{MAP}_{\text{BL}1}$, $\ln \text{MAP}_{\text{BL}2}$, $\ln \text{MAP}_{\text{MA}1}$, and $\ln \text{MAP}_{\text{MA}2}$) for each period were calculated to normalize the distribution.

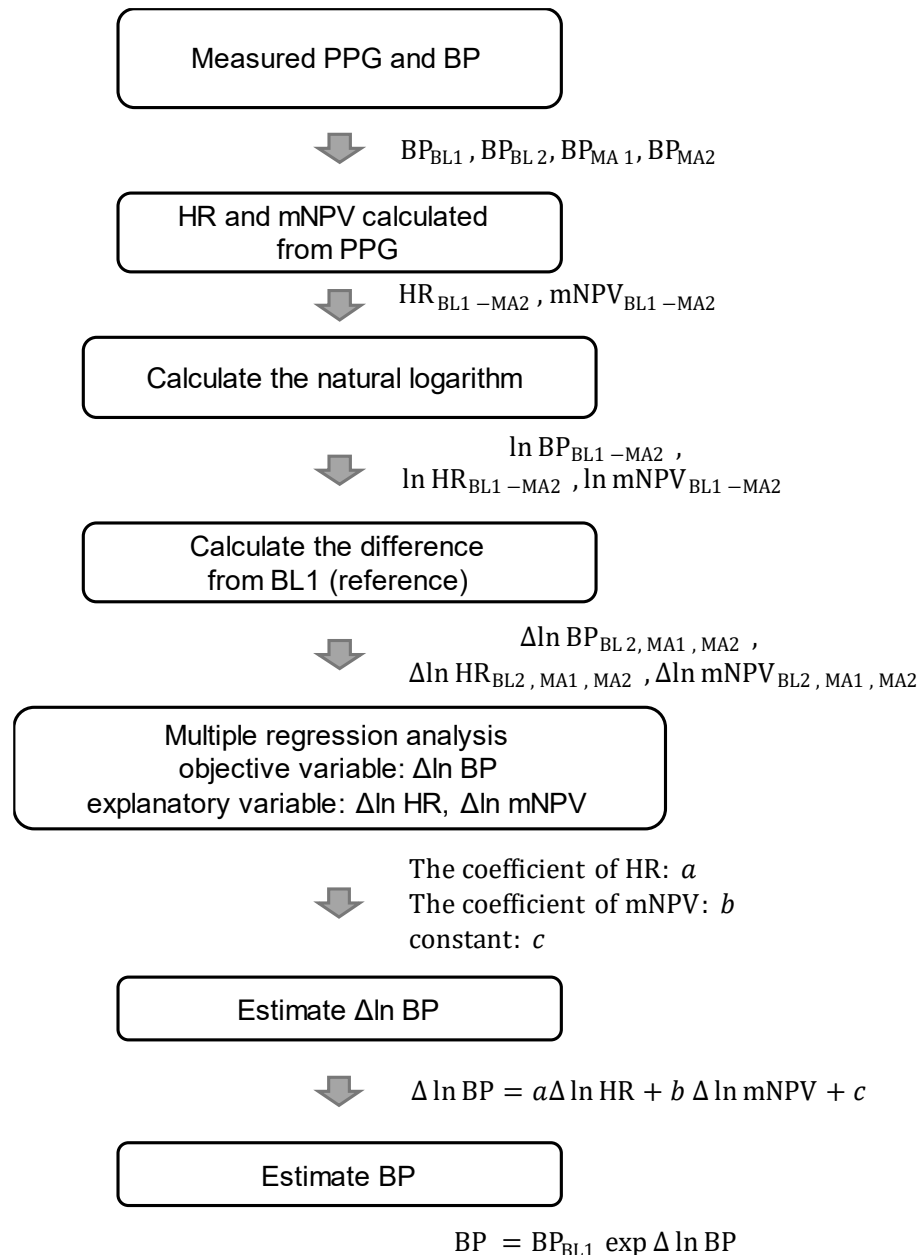


Figure 5. Flowchart of BP estimation. BP = blood pressure (SBP/DBP/MAP), HR = heart rate, and mNPV = modified normalized pulse volume.

Furthermore, to suppress individual differences, the difference values ($\Delta \ln \text{HR}$, $\Delta \ln \text{mNPV}$, $\Delta \ln \text{SBP}$, $\Delta \ln \text{DBP}$, and $\Delta \ln \text{MAP}$) for each value of BL2, MA1, and MA2 based on the value of BL1 were calculated, respectively, and used in the data analysis (e.g., $\Delta \ln$

$SBP_{MA1} = \ln SBP_{MA1} - \ln SBP_{BL1} = \ln(SBP_{MA1}/SBP_{BL1})$. Based on Equation (1), $\Delta \ln SBP$, $\Delta \ln DBP$, and $\Delta \ln MAP$ are expressed as follows [25]:

$$\text{Estimated } \Delta \ln SBP = a_{SBP} \Delta \ln HR + b_{SBP} \Delta \ln mNPV + c_{SBP}, \quad (2)$$

$$\text{Estimated } \Delta \ln DBP = a_{DBP} \Delta \ln HR + b_{DBP} \Delta \ln mNPV + c_{DBP}, \quad (3)$$

$$\text{Estimated } \Delta \ln MAP = a_{MAP} \Delta \ln HR + b_{MAP} \Delta \ln mNPV + c_{MAP}. \quad (4)$$

The values of the coefficients a , b , and c in Equations (2)–(4) were obtained using multiple linear regression analysis with $\Delta \ln SBP$, $\Delta \ln DBP$, and $\Delta \ln MAP$ as the objective variables and $\Delta \ln HR$ and $\Delta \ln mNPV$ as the explanatory variables. Via the natural exponential transformation (\exp) of Equations (2)–(4), the ratio of BP to the reference value BL1 was calculated (e.g., $\exp(\Delta \ln SBP_{MA1}) = SBP_{MA1}/SBP_{BL1}$). With this method, if the cuff sphygmomanometer value at BL1 is known, then the estimated BP for BL2, MA1, and MA2 can be obtained as the difference from the BP values obtained using Equations (2)–(4).

Therefore, by multiplying the known SBP_{BL1} , DBP_{BL1} , and MAP_{BL1} by the exponentially transformed estimated $\Delta \ln SBP$, $\Delta \ln DBP$, and $\Delta \ln MAP$, as in Equations (5)–(7), we obtain the estimated SBP, DBP, and MAP [25]:

$$\text{Estimated } SBP = SBP_{BL1} \exp(\text{Estimated } \Delta \ln SBP), \quad (5)$$

$$\text{Estimated } DBP = DBP_{BL1} \exp(\text{Estimated } \Delta \ln DBP), \quad (6)$$

$$\text{Estimated } MAP = MAP_{BL1} \exp(\text{Estimated } \Delta \ln MAP). \quad (7)$$

The estimation accuracy was evaluated by comparing the estimated values of SBP, DBP, and MAP with those measured with a cuff sphygmomanometer.

3. Results

Table 2 gives the mean values and standard deviations of the HR and mNPV obtained from the four measured PPG waveforms for each condition. These changes are statistically significant, which is reasonable because stress increases cardiac output and constricts peripheral blood vessels.

Table 2. Statistical results for HR and mNPV at 4 wavelengths in each condition.

Property	LED Color	Condition				Paired t-Test between BL and MA	
		BL		MA		<i>t</i>	<i>p</i>
		Mean	SD	Mean	SD		
HR [bpm]	Blue	72.8	12.7	89.8	15.8	-7.55	<0.001
	Green	72.8	12.7	89.5	15.7	-7.31	<0.001
	Red	72.7	12.5	88.6	15.2	-7.40	<0.001
	NIR	72.9	12.8	88.0	15.2	-6.45	<0.001
mNPV [a.u.]	Blue	0.0378	0.0179	0.0203	0.0074	6.28	<0.001
	Green	0.0364	0.0208	0.0193	0.0086	5.62	<0.001
	Red	0.0206	0.0104	0.0111	0.0041	4.80	<0.001
	NIR	0.0247	0.0115	0.0126	0.0047	5.84	<0.001

HR = heart rate, mNPV = modified normalized pulse volume, BL = baseline (resting condition), MA = mental arithmetic (stress condition induced via mental arithmetic), and $N = 14$.

The results of the multiple linear regression analysis using the $\Delta \ln MAP$, $\Delta \ln SBP$, and $\Delta \ln DBP$ measured with a cuff sphygmomanometer as the objective variables and the $\Delta \ln HR$ and $\Delta \ln mNPV$ calculated from the PPG at each wavelength as the explanatory variables are given in Table 3.

Table 3. Results of multiple linear regression analysis of BP estimation at each wavelength.

BP	LED Color	HR (a)				mNPV (b)				c
		R ²	p	B	std. β	p	β	std. β	p	
$\Delta \ln \text{SBP}$	Blue	0.612	<0.001	0.288	0.572	<0.001	-0.045	-0.262	0.079	-0.003
	Green	0.549	<0.001	0.337	0.661	<0.001	-0.022	-0.129	0.329	-0.003
	Red	0.592	<0.001	0.330	0.620	<0.001	-0.030	-0.209	0.122	-0.001
	NIR	0.634	<0.001	0.373	0.736	<0.001	-0.012	-0.086	0.520	0.001
$\Delta \ln \text{DBP}$	Blue	0.497	<0.001	0.203	0.280	0.097	-0.117	-0.475	0.006	0.024
	Green	0.406	<0.001	0.405	0.552	<0.001	-0.032	-0.134	0.375	0.021
	Red	0.48	<0.001	0.273	0.355	0.022	-0.084	-0.411	0.009	0.031
	NIR	0.47	<0.001	0.205	0.281	0.085	-0.097	-0.463	0.006	0.036
$\Delta \ln \text{MAP}$	Blue	0.630	<0.001	0.245	0.424	0.005	-0.084	-0.431	0.004	0.011
	Green	0.541	<0.001	0.377	0.646	<0.001	-0.028	-0.143	0.282	0.010
	Red	0.607	<0.001	0.303	0.497	<0.001	-0.059	-0.362	0.008	0.016
	NIR	0.598	<0.001	0.286	0.493	0.001	-0.058	-0.349	0.016	0.020

$\Delta \ln \text{BP} = a \times \Delta \ln \text{(heart rate (HR))} + b \times \Delta \ln \text{(modified normalized pulse volume (mNPV))} + \text{constant (c)}$. BP = blood pressure, SBP = systolic BP, DBP = diastolic BP, MAP = mean arterial pressure, NIR = near-infrared, R^2 = coefficient of determination, β = β coefficient of multiple linear regression, and std. β = standardized β .

As shown in Table 3, when comparing each wavelength in terms of the coefficient of determination (R^2), NIR shows the highest accuracy for $\Delta \ln \text{SBP}$, while blue shows the highest accuracy for both $\Delta \ln \text{DBP}$ and $\Delta \ln \text{MAP}$. For $\Delta \ln \text{SBP}$, although NIR has the best accuracy, blue also has a high accuracy of $R^2 = 0.612$. In addition, for $\Delta \ln \text{SBP}$ and $\Delta \ln \text{MAP}$, the accuracy of $R^2 > 0.5$ is excellent. Comparing each BP shows a trend of joint best accuracy for $\Delta \ln \text{SBP}$ and $\Delta \ln \text{MAP}$, followed by $\Delta \ln \text{DBP}$. Shapiro–Wilk tests did not detect a strong violation of the normality of the distribution in the residuals (all p -values were >0.011).

Scatter plots of the measured $\Delta \ln \text{SBP}$, measured $\Delta \ln \text{DBP}$, and measured $\Delta \ln \text{MAP}$ obtained using the cuff sphygmomanometer and the estimated $\Delta \ln \text{SBP}$, estimated $\Delta \ln \text{DBP}$, and estimated $\Delta \ln \text{MAP}$ at each wavelength are shown in Figures 6–8, and Bland–Altman plots are shown in Figures 9–11. In addition, Table 4 summarizes the means and standard deviations of the differences between the BP values measured with a cuff sphygmomanometer and the estimated BP values, and the number of data when the error is divided into 4 classes: 0–5, 5–10, 10–15, and $>15 \text{ mmHg}$. Figures 9–11 and Table 4 show that most of the values are within the limits of agreement, which indicates that the BP estimated using this method agrees well with the measured BP regardless of the wavelength.

Table 4. Difference between estimated BP and measured BP with a cuff sphygmomanometer.

	SBP				DBP				MAP			
	B	G	R	NIR	B	G	R	NIR	B	G	R	NIR
Mean (mmHg)	4.84	5.27	4.90	4.67	4.68	5.13	5.00	5.01	3.57	4.09	3.98	3.97
SD (mmHg)	3.83	4.20	4.06	3.79	4.60	4.84	4.25	4.42	4.01	4.28	3.71	3.86
0–5 mmHg	24	22	25	26	27	26	27	27	32	29	31	32
5–10 mmHg	12	15	13	13	10	11	8	10	6	8	7	6
10–15 mmHg	6	3	2	2	3	2	6	4	3	3	3	3
>15 mmHg	0	2	2	1	2	3	1	1	1	2	1	1

BP = blood pressure; SBP = systolic BP; DBP = diastolic BP; MAP = mean arterial pressure; B = blue LED; G = green LED; R = red LED; NIR = near-infrared LED; mean = average difference between measured BP and estimated BP; SD = standard deviation of difference between measured BP and estimated BP; and 0–5, 5–10, 10–15, and $>15 \text{ mmHg}$: number of data when the error is divided into 4 classes.

Table 5 shows the means and standard deviations of each estimated BP from the PPG for each condition. Regardless of the wavelength, DBP, SBP, and MAP increased in the MA condition compared with BL. This difference in BP was statistically significant and was consistent with the trend of BP measured with a cuff sphygmomanometer. Therefore, changes in BP were captured using the BP estimated with this method.

Table 5. Statistical results of estimated BP at 4 wavelengths in each condition.

Property	LED Color	Condition				Paired <i>t</i> -Test between BL and MA	
		BL		MA		<i>t</i>	<i>p</i>
		Mean	SD	Mean	SD		
SBP [mmHg]	Blue	111.6	13.2	122.3	14.4	-7.85	<0.001
	Green	112.0	13.4	122.1	14.3	-8.16	<0.001
	Red	111.9	13.2	122.2	13.9	-7.69	<0.001
	NIR	112.2	13.2	122.0	14.0	-6.85	<0.001
DBP [mmHg]	Blue	69.3	6.5	78.0	7.8	-7.22	<0.001
	Green	69.8	6.6	77.8	8.2	-7.89	<0.001
	Red	69.4	6.1	77.9	7.5	-7.38	<0.001
	NIR	69.3	6.2	77.9	7.3	-8.21	<0.001
MAP [mmHg]	Blue	83.4	7.6	92.7	8.9	-7.62	<0.001
	Green	83.9	7.7	92.6	9.0	-8.07	<0.001
	Red	83.5	7.3	92.7	8.3	-7.67	<0.001
	NIR	83.6	7.6	92.6	8.5	-8.16	<0.001

BP = blood pressure, SBP = systolic BP, DBP = diastolic BP, MAP = mean arterial pressure, BL = baseline (resting condition), MA = mental arithmetic (stress condition induced via mental arithmetic), and $N = 14$.

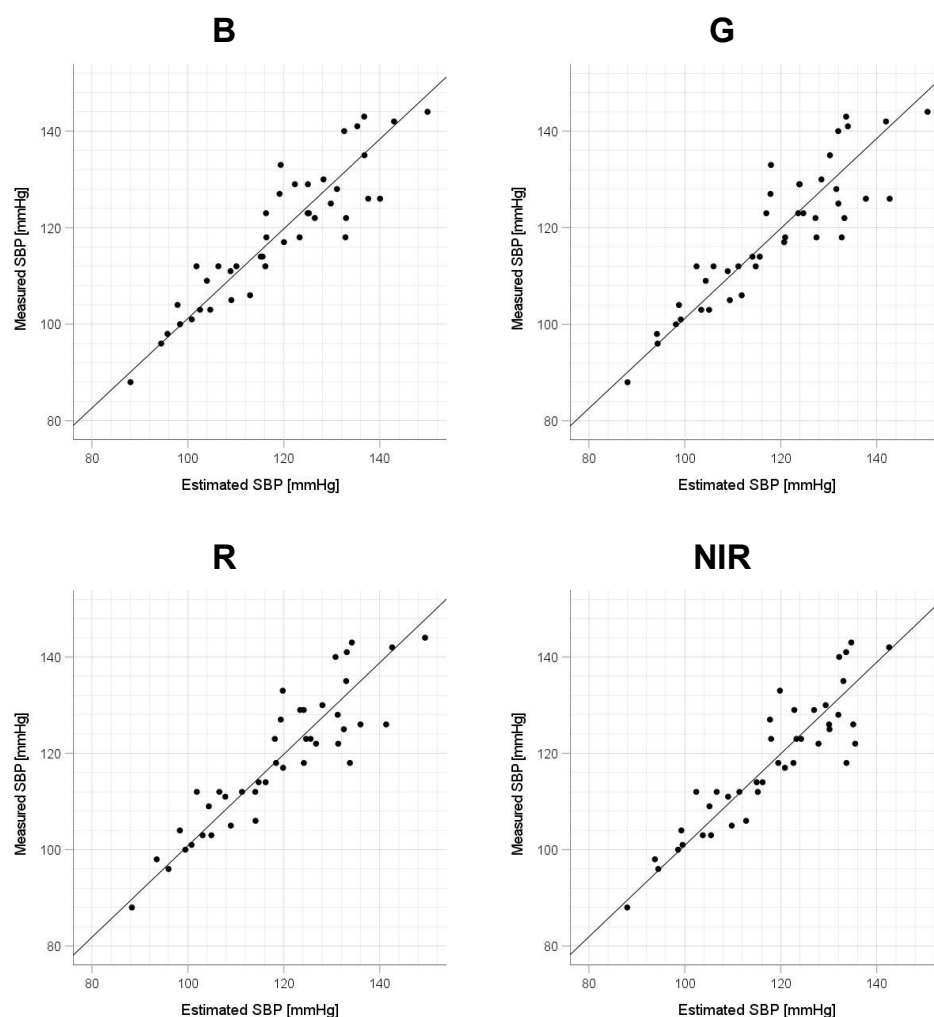


Figure 6. Accuracy of systolic blood pressure (SBP) estimation at each wavelength. Scatterplots of SBP estimated using proposed method and SBP measured with a cuff sphygmomanometer ($N = 42$). From left to right, the light source wavelengths are blue (B), green (G), red (R), and near-infrared (NIR). The solid line on each scatterplot is the regression line with geometric mean regression.

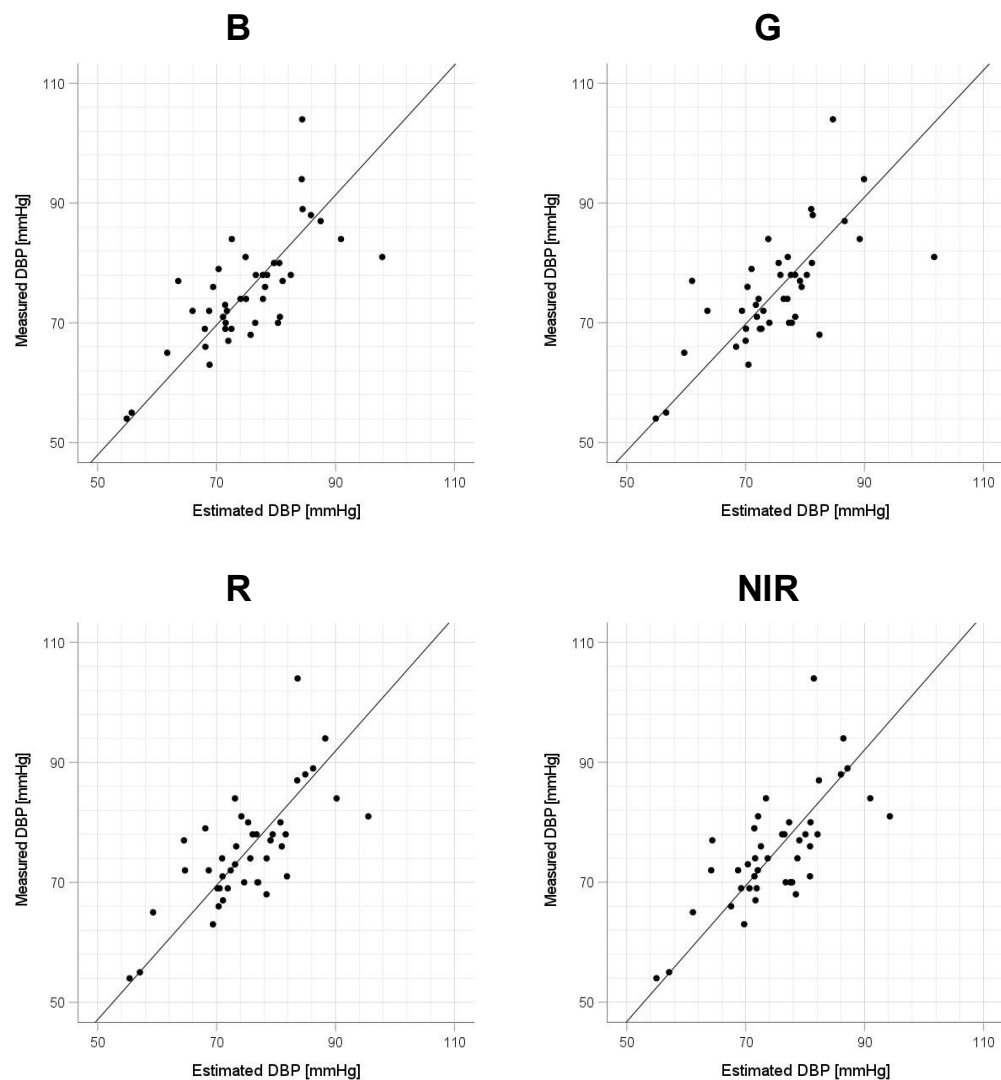


Figure 7. Accuracy of diastolic blood pressure (DBP) estimation at each wavelength. Scatterplots of DBP estimated using proposed method and DBP measured with a cuff sphygmomanometer ($N = 42$). From left to right, the light source wavelengths are blue (B), green (G), red (R), and near-infrared (NIR). The solid line on each scatterplot is the regression line with geometric mean regression.

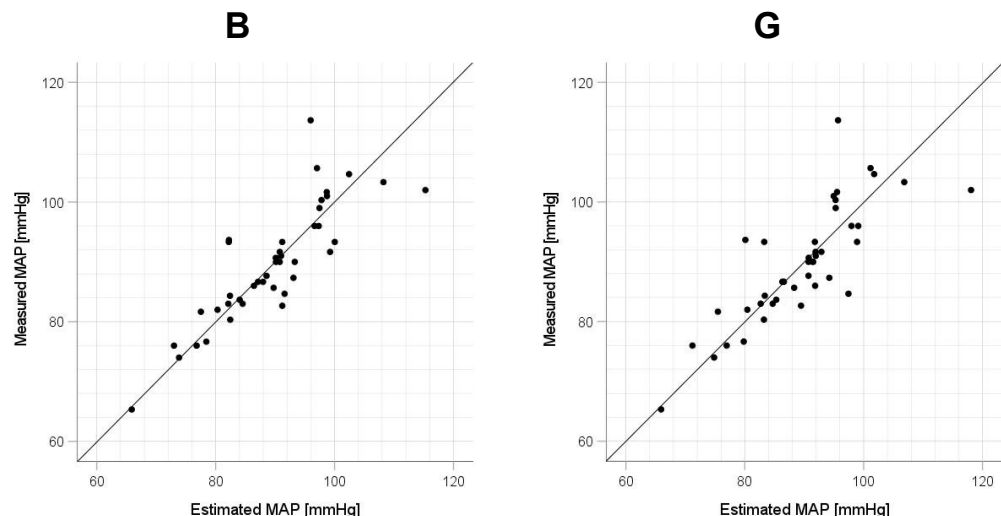


Figure 8. Cont.

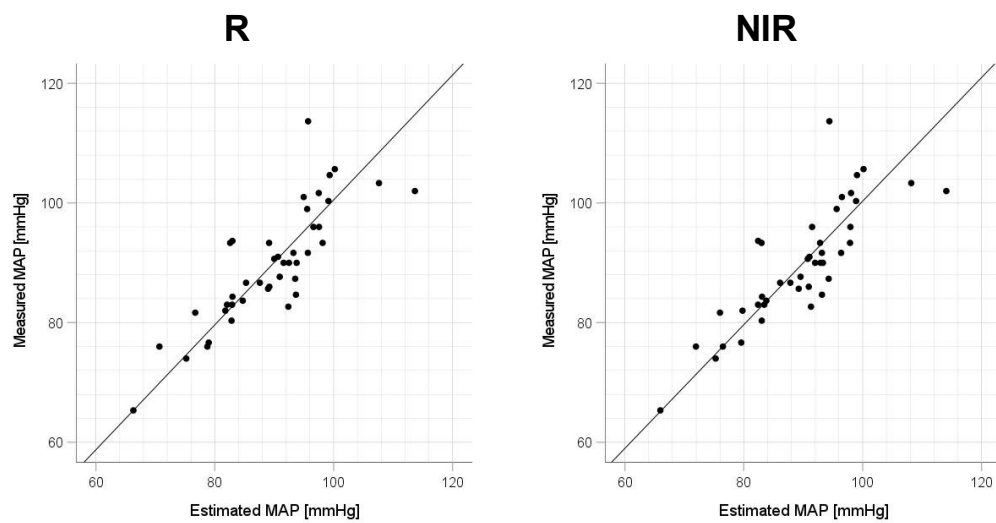


Figure 8. Accuracy of mean arterial pressure (MAP) estimation at each wavelength. Scatterplots of MAP estimated using proposed method and MAP measured with a cuff sphygmomanometer ($N = 42$). From left to right, the light source wavelengths are blue (B), green (G), red (R), and near-infrared (NIR). The solid line on each scatterplot is the regression line with geometric mean regression.

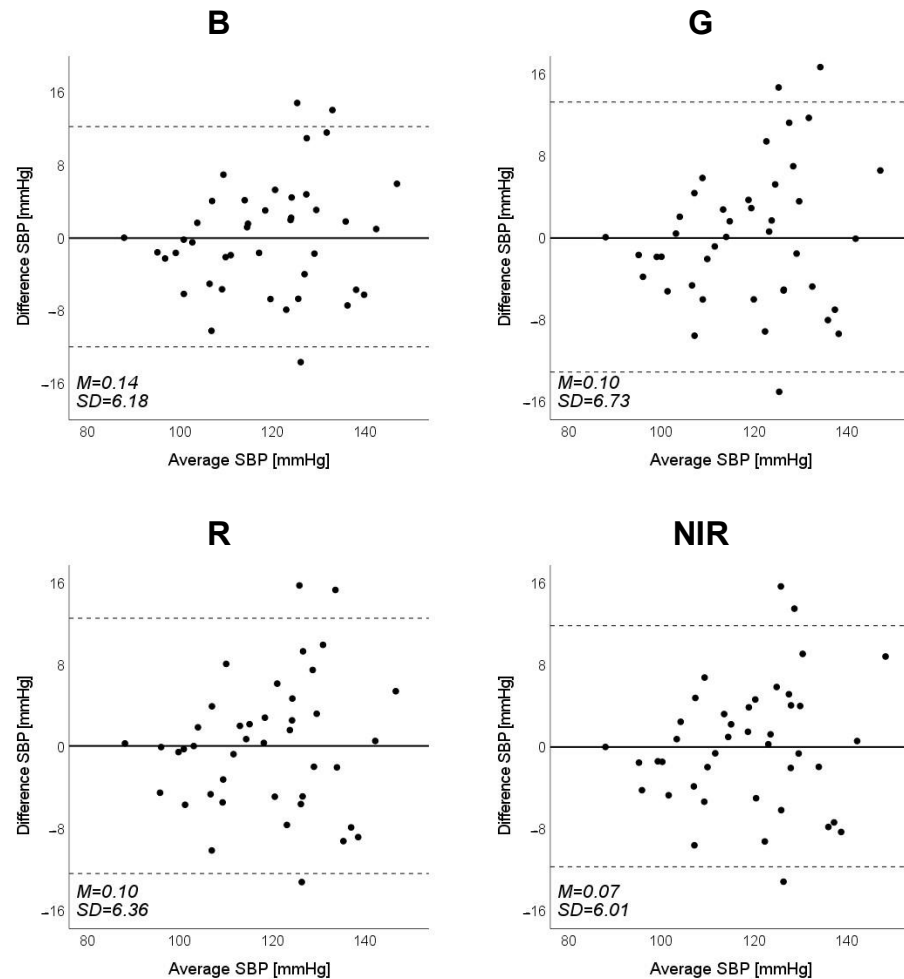


Figure 9. Bland–Altman plots of estimated systolic blood pressure (SBP) against those measured with a cuff sphygmomanometer ($N = 42$). From left to right, the light source is blue (B), green (G), red (R), and near-infrared (NIR). The solid line and the dashed lines on each plot represent fixed bias (M) and $M \pm 1.96$ standard deviation range, respectively.

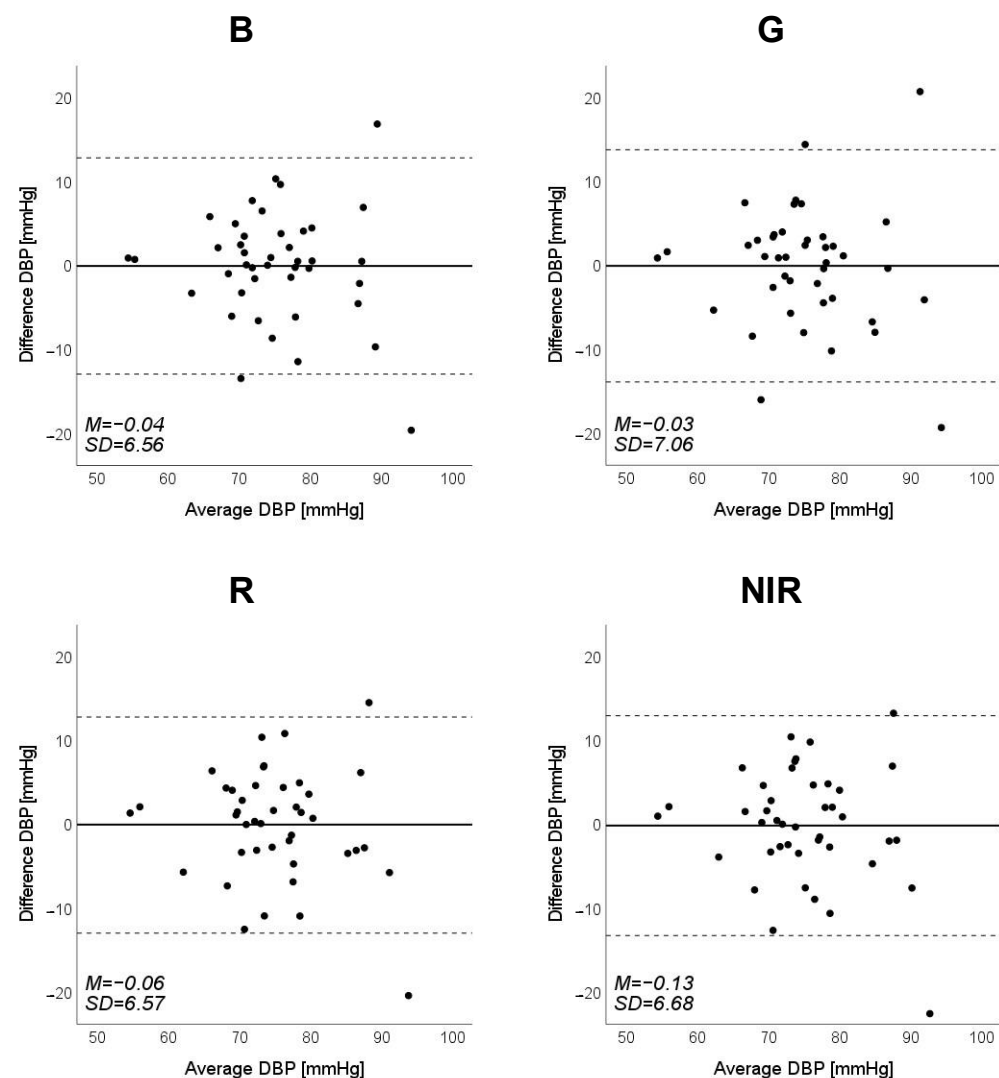


Figure 10. Bland–Altman plots of estimated diastolic blood pressure (DBP) against those measured with a cuff sphygmomanometer ($N = 42$). From left to right, the light source is blue (B), green (G), red (R), and near-infrared (NIR). The solid line and the dashed lines on each plot represent fixed bias (M) and $M \pm 1.96$ standard deviation range, respectively.

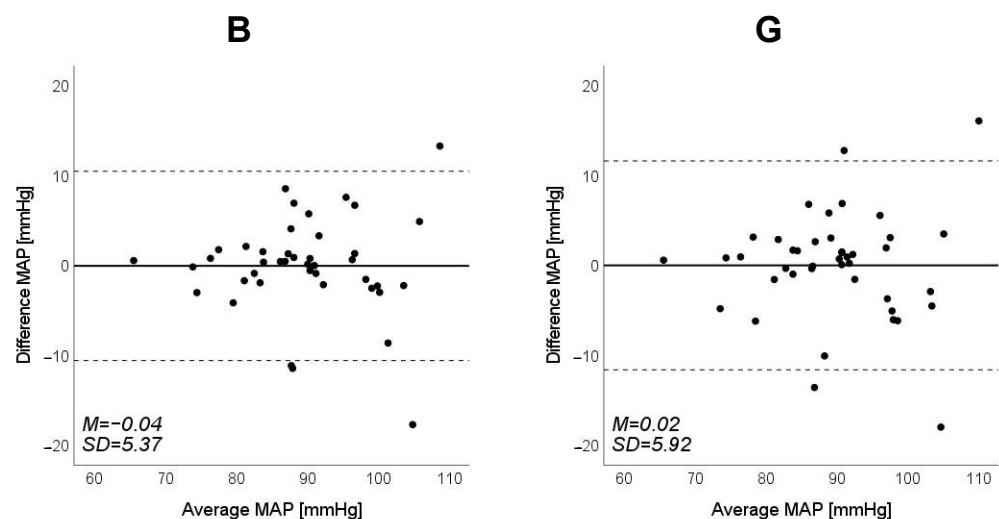


Figure 11. Cont.

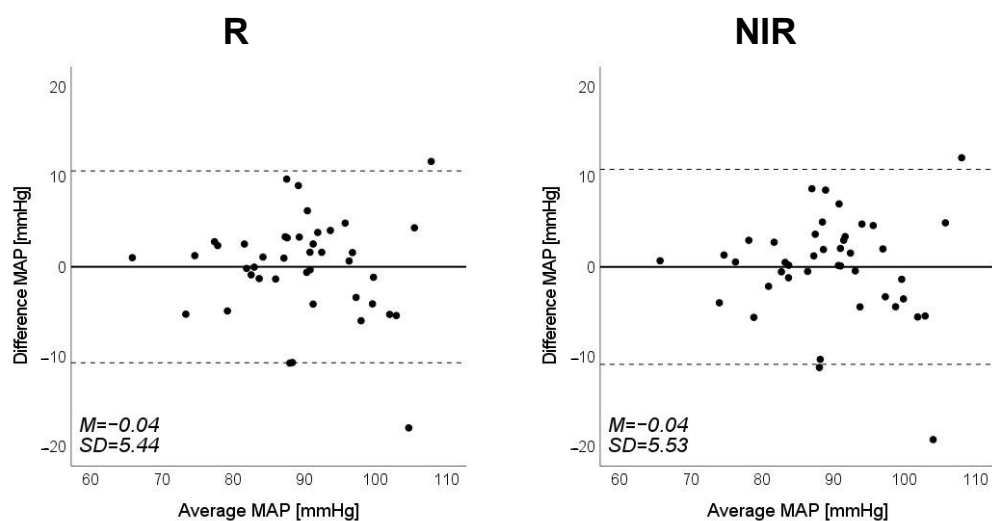


Figure 11. Bland–Altman plots of estimated mean arterial pressure (MAP) against those measured with a cuff sphygmomanometer ($N = 42$). From left to right, the light source is blue (B), green (G), red (R), and near-infrared (NIR). The solid line and the dashed lines on each plot represent fixed bias (M) and $M \pm 1.96$ standard deviation range, respectively.

4. Discussion

In Table 6, we focus on the wavelengths of the LEDs, having obtained the means of the R^2 values for the three types of BP (DBP, SBP, and MAP) and compared them using a one-way repeated measures analysis of variance (ANOVA). For post hoc comparison, we used Tukey's honestly significant difference (HSD) test for multiple comparisons. The one-way repeated measures ANOVA revealed the main effect of type, $F(3,6) = 18.74$, $p = 0.002$. The subsequent post hoc Tukey's HSD test for multiple comparisons revealed that the mean R^2 of green was less than that of blue, red, and NIR. This result indicates that wavelengths other than green should be used as the light source with this method. The inferiority of green LEDs is due to the low R^2 of DBP, which is clearly dependent on the TPR [39]. Therefore, the measurement of the mNPV, which is correlated with the TPR, may lack accuracy. This may be due to a problem with the vessels that are captured at the depth of arrival of the green light.

Table 6. Coefficient of determination at each wavelength of PPG and results of statistical tests.

	LED Color						Results of Statistical Tests				
	B		G		R		NIR		ANOVA		
	Mean	SD	Mean	SD	Mean	SD	Mean	SD	$F(3,6)$	p	Tukey's HSD
R^2	0.580	0.059	0.499	0.066	0.560	0.057	0.567	0.070	18.74	0.002	G < B, R, NIR

R^2 = coefficient of determination, B = blue LED, G = green LED, R = red LED, NIR = near-infrared LED, and HSD = honestly significant difference.

Focusing on the R^2 values in Table 3, we consider the optimal wavelengths for SBP, DBP, and MAP. For SBP, NIR is the optimal wavelength because of its largest R^2 ($=0.634$) in the order of NIR $>$ blue $>$ red $>$ green. Similarly, for DBP and MAP, the order is blue $>$ NIR $>$ red $>$ green, so blue is the optimal wavelength ($R^2 = 0.497$ for DBP and $R^2 = 0.630$ for MAP). However, these differences were not statistically significant. Furthermore, we focus on the values of the standard partial regression coefficient (std. β) of the β coefficients for HR (a) and mNPV (b) at the optimal wavelengths (SBP: NIR; DBP and MAP: blue) in Table 3. For SBP, the coefficient a was larger than b for std. β . For DBP, b was larger than a . For MAP, a and b were about the same. Previous studies have shown that HR depends on CO in SBP [40,41], TPR in DBP [41], and CO and TPR in MAP [14]. Because

CO and TPR are associated with HR and mNPV, respectively [28–32], the trend of std. β , whereby the a of HR is dominant in SBP and the b of mNPV is dominant in DBP, agrees well with physiological trends.

In this study, the optimal wavelengths for SBP, DBP, and MAP were different, which is likely because of the differences in the optical properties of biological tissues. The depth to which light penetrates biological tissue differs depending on wavelength, with longer-wavelength light penetrating deeper. Regarding the wavelengths used in this study, blue, green, red, and NIR reach deeper in that order, such that NIR can reach deep blood vessels, whereas blue can only reach peripheral ones in the epidermis. Therefore, using NIR gives information about relatively large blood vessels in deep areas, which have large changes in blood vessel volume, and the HR can be obtained with high accuracy; however, the information about peripheral blood vessels in the epidermis is lost among that about deep vessels. On the other hand, because blue reaches only the epidermis, it is thought that using it produces PPGs that reflect well the information about peripheral vessels. Therefore, we reason that NIR, which is better at measuring HR, and blue, which is better at measuring mNPV, can estimate SBP and DBP more accurately, respectively. For MAP, both blue and NIR are highly accurate, but in this study, at least among the participants before the experiment, the intensity of light emitted from the body was set to be constant at each wavelength, so the difference in the accuracy of the HR obtained from the PPG at each wavelength was lower while that of the blue estimation was higher. In other words, if a light source is available that can emit sufficiently strong light, then blue is the optimal wavelength for this method. Based on the above results, although no statistically significant difference was found for the trend of the present results, we believe that the results have a certain significance when physiological and optical characteristics are considered.

This study has several limitations. First, the participants were relatively few in number and included only healthy Japanese men and women of approximately the same age; therefore, the effects of the age, skin color, and health status of the participants require further investigation. Regarding the small number of data, we note that this study is at the stage of basic investigation and not at the stage of attempting practical application. Second, the participants were measured only while physically still, but it is known that PPGs are strongly affected by motion artifacts and that the effect varies depending on the wavelength of the light source [42]; therefore, for this method to be used in practice, it is necessary to investigate the extent to which the measurement accuracy is degraded and whether the optimum wavelength is changed in an environment in which body motion occurs. To address the small number of participants and the age bias in this study, in future work, it will be necessary to conduct experiments with a large number of participants and a wider range of ages to determine whether the results are statistically significant. Figures 6–8 show that the error tends to be larger when blood pressure is higher. To realize the practical application of the proposed method, further improvements in accuracy are needed, including this point. If these problems can be solved, the proposed method is expected to be a useful method for performing simple blood pressure estimation.

Despite the above limitations, we have proposed a BP estimation method that requires only a simple PPG sensor, unlike a cuff sphygmomanometer or methods that require PPGs and ECGs. Furthermore, we have clarified the differences in the measurement accuracy due to the differences in light source wavelengths, which have not been considered to date.

5. Conclusions

In this study, we investigated the optimal light source wavelength for cuffless BP estimation using only the HR and mNPV obtained from PPGs. Using a PPG sensor capable of measuring PPGs simultaneously at four different wavelengths, we evaluated the accuracy of the estimation by performing multiple regression analysis on the HR and mNPV at each wavelength obtained for the SBP, DBP, and MAP measured both from the PPGs and using

a cuff sphygmomanometer. From the results, although not significant, NIR was found to be the most accurate wavelength for SBP, and blue was found to be that for DBP and MAP. These results are consistent with physiological findings and indicate that the light source wavelength will become an important factor in cuffless BP estimation using PPGs in the future and that the accuracy of BP estimation can be improved by selecting the optimal wavelength according to the type of blood pressure.

Author Contributions: Conceptualization, S.T. and K.M.; methodology, S.T. and K.M.; formal analysis, K.M.; investigation, S.T.; data curation, S.T. and K.M.; writing—original draft preparation, S.T.; writing—review and editing, K.M.; project administration, K.M.; funding acquisition, S.T. All authors have read and agreed to the published version of the manuscript.

Funding: This research was funded by the Tateisi Science and Technology Foundation, grant number 2201015, and JSPS KAKENHI, grant number JP18K12070.

Institutional Review Board Statement: This study was conducted in accordance with the Declaration of Helsinki and approved by the Institutional Ethics Committee of the National Institute of Technology, Ishikawa College (protocol code: N.A.; 13 November 2019).

Informed Consent Statement: Informed consent was obtained from all subjects involved in this study.

Data Availability Statement: The data supporting the findings of this study, except for the raw data, are available via e-mail from the corresponding author upon reasonable request.

Acknowledgments: The authors would like to thank Mizuki Muramoto (National Institute of Technology, Ishikawa College) for her assistance in conducting this experiment.

Conflicts of Interest: The authors declare no conflict of interest.

References

1. James, P.A.; Oparil, S.; Carter, B.L.; Cushman, W.C.; Dennison-Himmelfarb, C.; Handler, J.; Lackland, D.T.; LeFevre, M.L.; MacKenzie, T.D.; Ogedegbe, O.; et al. 2014 evidence-based guideline for the management of high blood pressure in adults: Report from the panel members appointed to the Eighth Joint National Committee (JNC 8). *JAMA* **2014**, *311*, 507–520. [[CrossRef](#)]
2. Parati, G.; Ochoa, J.E.; Lombardi, C.; Bilo, G. Assessment and management of blood-pressure variability. *Nat. Rev. Cardiol.* **2013**, *10*, 143–155. [[CrossRef](#)]
3. Burnier, M.; Egan, B.M. Adherence in Hypertension. *Circ. Res.* **2019**, *124*, 1124–1140. [[CrossRef](#)]
4. Johansson, J.K.; Niiranen, T.J.; Puukka, P.J.; Jula, A.M. Prognostic value of the variability in home-measured blood pressure and heart rate: The Finn-Home Study. *Hypertension* **2012**, *59*, 212–218. [[CrossRef](#)]
5. Hansen, T.W.; Thijs, L.; Li, Y.; Boggia, J.; Kikuya, M.; Björklund-Bodegård, K.; Richart, T.; Ohkubo, T.; Jeppesen, J.; Torp-Pedersen, C.; et al. Prognostic value of reading-to-reading blood pressure variability over 24 hours in 8938 subjects from 11 populations. *Hypertension* **2010**, *55*, 1049–1057. [[CrossRef](#)]
6. Yamakoshi, K.; Shimazu, H.; Shibata, M.; Kamiya, A. New oscillometric method for indirect measurement of systolic and mean arterial pressure in the human finger. Part 1: Model experiment. *Med. Biol. Eng. Comput.* **1982**, *20*, 307–313. [[CrossRef](#)]
7. Kaplan, N.M.; Victor, R.G. Chapter 2 Measurement of Blood Pressure. In *Kaplan's Clinical Hypertension*, 11th ed.; LWW: Philadelphia, PA, USA, 2014; pp. 18–39.
8. Mukkamala, R.; Hahn, J.O.; Inan, O.T.; Mestha, L.K.; Kim, C.S.; Töreyin, H.; Kyal, S. Toward Ubiquitous Blood Pressure Monitoring via Pulse Transit Time: Theory and Practice. *IEEE Trans. Biomed. Eng.* **2015**, *62*, 1879–1901. [[CrossRef](#)]
9. Sharma, M.; Barbosa, K.; Ho, V.; Griggs, D.; Ghirmai, T.; Krishnan, S.K.; Hsiai, T.K.; Chiao, J.-C.; Cao, H. Cuff-less and continuous blood pressure monitoring: A methodological review. *Technologies* **2017**, *5*, 21. [[CrossRef](#)]
10. Wibmer, T.; Doering, K.; Kropf-Schenk, C.; Rüdiger, S.; Blanta, I.; Stoiber, K.M.; Rottbauer, W.; Schumann, C. Pulse transit time and blood pressure during cardiopulmonary exercise tests. *Physiol. Res.* **2014**, *63*, 287–296. [[CrossRef](#)]
11. Proença, J.; Muehlsteff, J.; Aubert, X.; Carvalho, P. Is pulse transit time a good indicator of blood pressure changes during short physical exercise in a young population? *Annu. Int. Conf. IEEE Eng. Med. Biol. Soc.* **2010**, *2010*, 598–601. [[CrossRef](#)]
12. Fung, P.; Dumont, G.; Ries, C.; Mott, C.; Ansermino, M. Continuous noninvasive blood pressure measurement by pulse transit time. *Conf. Proc. IEEE Eng. Med. Biol. Soc.* **2004**, *2006*, 738–741. [[CrossRef](#)]
13. Choi, Y.; Zhang, Q.; Ko, S. Noninvasive cuffless blood pressure estimation using pulse transit time and Hilbert–Huang transform. *Comput. Electr. Eng.* **2013**, *39*, 103–111. [[CrossRef](#)]
14. Kumar, N.; Agrawal, A.; Deb, S. Cuffless BP measurement using a correlation study of pulse transient time and heart rate. In Proceedings of the 2014 International Conference on Advances in Computing, Communications and Informatics (ICACCI), Delhi, India, 24–27 September 2014; IEEE: Piscataway, NJ, USA; pp. 1538–1541. [[CrossRef](#)]

15. Payne, R.A.; Symeonides, C.N.; Webb, D.J.; Maxwell, S.R. Pulse transit time measured from the ECG: An unreliable marker of beat-to-beat blood pressure. *J. Appl. Physiol.* **1985**, *2006*, 100, 136–141. [[CrossRef](#)]
16. Patzak, A.; Mendoza, Y.; Gesche, H.; Konermann, M. Continuous blood pressure measurement using the pulse transit time: Comparison to intra-arterial measurement. *Blood Press.* **2015**, *24*, 217–221. [[CrossRef](#)]
17. Gesche, H.; Grosskurth, D.; Küchler, G.; Patzak, A. Continuous blood pressure measurement by using the pulse transit time: Comparison to a cuff-based method. *Eur. J. Appl. Physiol.* **2012**, *112*, 309–315. [[CrossRef](#)]
18. Barvik, D.; Cerny, M.; Penhaker, M.; Noury, N. Noninvasive Continuous Blood Pressure Estimation From Pulse Transit Time: A Review of the Calibration Models. *IEEE Rev. Biomed. Eng.* **2022**, *15*, 138–151. [[CrossRef](#)]
19. Chua, C.P.; Heneghan, C. Continuous blood pressure monitoring using ECG and finger photoplethysmogram. *Conf. Proc. IEEE Eng. Med. Biol. Soc.* **2006**, *2006*, 5117–5120. [[CrossRef](#)]
20. Samria, R.; Jain, R.; Jha, A.; Saini, S.; Chowdhury, S.R. Noninvasive cuff’less estimation of blood pressure using Photoplethysmography without electrocardiograph measurement. In *2014 IEEE Region 10 Symposium*; IEEE: Piscataway, NJ, USA, 2014; pp. 254–257. [[CrossRef](#)]
21. Li, Z.; He, W. A Continuous Blood Pressure Estimation Method Using Photoplethysmography by GRNN-Based Model. *Sensor* **2021**, *21*, 7207. [[CrossRef](#)]
22. Maher, N.; Elsheikh, G.; Anis, W.R.; Emara, T. Non-invasive calibration-free blood pressure estimation based on artificial neural network. In *International Conference on Advanced Machine Learning Technologies and Applications*; Springer: Berlin/Heidelberg, Germany, 2019; pp. 701–711. [[CrossRef](#)]
23. Chandrasekhar, A.; Kim, C.S.; Naji, M.; Natarajan, K.; Hahn, J.O.; Mukkamala, R. Smartphone-based blood pressure monitoring via the oscillometric finger-pressing method. *Sci. Transl. Med.* **2018**, *10*, eaap8674. [[CrossRef](#)]
24. Yamakoshi, T.; Rolfe, P.; Yamakoshi, K.I. Cuffless blood pressure estimation based on haemodynamic principles: Progress towards mobile healthcare. *PeerJ* **2021**, *9*, e11479. [[CrossRef](#)]
25. Matsumura, K.; Rolfe, P.; Toda, S.; Yamakoshi, T. Cuffless blood pressure estimation using only a smartphone. *Sci. Rep.* **2018**, *8*, 7298. [[CrossRef](#)] [[PubMed](#)]
26. Geddes, L.A.; Voelz, M.H.; Babbs, C.F.; Bourland, J.D.; Tacker, W.A. Pulse transit time as an indicator of arterial blood pressure. *Psychophysiology* **1981**, *18*, 71–74. [[CrossRef](#)] [[PubMed](#)]
27. Guyton, A.C.; Hall, J.E. *Human Physiology and Mechanisms of Disease*, 6th ed.; Saunders: Philadelphia, PA, USA, 1986.
28. Gregg, M.E.; Matyas, T.A.; James, J.E. A new model of individual differences in hemodynamic profile and blood pressure reactivity. *Psychophysiology* **2002**, *39*, 64–72. [[CrossRef](#)] [[PubMed](#)]
29. Sherwood, A.; Dolan, C.A.; Light, K.C. Hemodynamics of blood pressure responses during active and passive coping. *Psychophysiology* **1990**, *27*, 656–668. [[CrossRef](#)] [[PubMed](#)]
30. Lee, J.; Matsumura, K.; Yamakoshi, T.; Rolfe, P.; Tanaka, N.; Kim, K.; Yamakoshi, K. Validation of normalized pulse volume in the outer ear as a simple measure of sympathetic activity using warm and cold pressor tests: Towards applications in ambulatory monitoring. *Physiol. Meas.* **2013**, *34*, 359–375. [[CrossRef](#)]
31. Matsumura, K.; Shimizu, K.; Rolfe, P.; Kakimoto, M.; Yamakoshi, T. Inter-method reliability of pulse volume related measures derived using finger-photoplethysmography: Across sensor positions and light intensities. *J. Psychophysiol.* **2018**, *32*, 182. [[CrossRef](#)]
32. Sawada, Y.; Tanaka, G.; Yamakoshi, K.I. Normalized pulse volume (NPV) derived photo-plethysmographically as a more valid measure of the finger vascular tone. *Int. J. Psychophysiol.* **2001**, *41*, 1–10. [[CrossRef](#)] [[PubMed](#)]
33. Anderson, R.R.; Parrish, J.A. The optics of human skin. *J. Investig. Derm.* **1981**, *77*, 13–19. [[CrossRef](#)]
34. Roggan, A.; Friebel, M.; Do Rschel, K.; Hahn, A.; Mu Ller, G. Optical Properties of Circulating Human Blood in the Wavelength Range 400–2500 nm. *J. Biomed. Opt.* **1999**, *4*, 36–46. [[CrossRef](#)]
35. Bashkatov, A.N.; Genina, E.; Kochubey, V.; Tuchin, V. Optical properties of human skin, subcutaneous and mucous tissues in the wavelength range from 400 to 2000 nm. *J. Phys. D Appl. Phys.* **2005**, *38*, 2543. [[CrossRef](#)]
36. Allen, J. Photoplethysmography and its application in clinical physiological measurement. *Physiol. Meas.* **2007**, *28*, R1–R39. [[CrossRef](#)] [[PubMed](#)]
37. Kamal, A.; Harness, J.; Irving, G.; Mearns, A. Skin photoplethysmography—A review. *Comput. Methods Programs Biomed.* **1989**, *28*, 257–269. [[CrossRef](#)]
38. Whelton, P.K.; Carey, R.M.; Aronow, W.S.; Casey, D.E.; Collins, K.J.; Dennison Himmelfarb, C.; DePalma, S.M.; Gidding, S.; Jamerson, K.A.; Jones, D.W.; et al. 2017 ACC/AHA/AAPA/ABC/ACPM/AGS/APhA/ASH/ASPC/NMA/PCNA Guideline for the Prevention, Detection, Evaluation, and Management of High Blood Pressure in Adults: A Report of the American College of Cardiology/American Heart Association Task Force on Clinical Practice Guidelines. *Circulation* **2018**, *138*, e484–e594. [[CrossRef](#)] [[PubMed](#)]
39. Protopgerou, A.D.; Safar, M.E.; Iaria, P.; Safar, H.; Le Dugal, K.; Filipovsky, J.; Henry, O.; Ducimetière, P.; Blacher, J. Diastolic blood pressure and mortality in the elderly with cardiovascular disease. *Hypertension* **2007**, *50*, 172–180. [[CrossRef](#)] [[PubMed](#)]
40. Light, K.C. Young Psychophysiologist Award address, 1980. Cardiovascular responses to effortful active coping: Implications for the role of stress in hypertension development. *Psychophysiology* **1981**, *18*, 216–225. [[CrossRef](#)] [[PubMed](#)]

41. Obrist, P.A.; Gaebelein, C.J.; Teller, E.S.; Langer, A.W.; Grignolo, A.; Light, K.C.; McCubbin, J.A. The relationship among heart rate, carotid dP/dt, and blood pressure in humans as a function of the type of stress. *Psychophysiology* **1978**, *15*, 102–115. [[CrossRef](#)] [[PubMed](#)]
42. Matsumura, K.; Toda, S.; Kato, Y. RGB and near-infrared light reflectance/transmittance photoplethysmography for measuring heart rate during motion. *IEEE Access* **2020**, *8*, 80233–80242. [[CrossRef](#)]

Disclaimer/Publisher’s Note: The statements, opinions and data contained in all publications are solely those of the individual author(s) and contributor(s) and not of MDPI and/or the editor(s). MDPI and/or the editor(s) disclaim responsibility for any injury to people or property resulting from any ideas, methods, instructions or products referred to in the content.